Development of an Al 7050-10 vol.% alumina nanocomposite through cold consolidation of particles by high-pressure torsion

Fabio R. Milhorato[a], Roberto B. Figueiredo[a], Terence G. Langdon[b], Eric M. Mazzer[a]

[a]Department of Metallurgical and Materials Engineering, Universidade Federal de Minas Gerais, Belo Horizonte, MG 31270-901, Brazil

[b]Materials Research Group, Department of Mechanical Engineering, University of Southampton, Southampton, SO17 1BJ, UK

Abstract

An Al 7050-10 vol.% Al_2O_3 nanocomposite was produced by cold consolidation of Al 7050 gas-atomized powder with alumina particles by means of severe plastic deformation using high-pressure torsion (HPT). The processing was conducted at room temperature under a pressure of 6.0 GPa, for 50 revolutions with a rotation speed of 2 rpm. The purpose of this work was to consolidate at room temperature one high strength Al alloy with Al_2O_3 particles without any prior or post sintering. In order to characterize the product, the disk microstructure was examined after consolidation using scanning and transmission electron microscopy and X-ray diffraction was used to determine the presence of different phases. Energy-dispersive X-ray spectroscopy (EDS) was undertaken to provide chemical analysis of the phases and hardness tests were performed to check the strength. The results show that the alumina particles in the periphery of the disk are more finely dispersed than in the central regions. The average grain size of the Al 7050 matrix ranged from ~50 to ~200 nm and the hardness measurements varied from ~237 Hv to ~307 Hv with disk edges having higher hardness values than in the central area.

Keywords: aluminum alloy; consolidation; high-pressure torsion; nanocomposite; severe plastic deformation

1. Introduction

The 7xxx series Al alloys are precipitation hardening Al-Zn–Mg–(Cu) alloys with a vast number of applications in the aerospace industry where the aircraft structures are subjected to demanding operating conditions and must comply with rigorous safety and performance requirements [1]. The important necessary properties for these applications, such as high strength, ductility, corrosion resistance and damage tolerance (e.g. fracture toughness and fatigue resistance), can be achieved by appropriate processing and alloying [2].

An interesting route for improving the mechanical properties of aluminum alloys, and a route that has drawn significant attention from researchers and industry, is the incorporation of hard reinforcement phases within the matrix, mostly in the form of ceramics, to produce metal matrix composites (MMCs). As with most composite materials, the addition of second phase particles leads to significantly enhanced properties by comparison with conventional monolithic materials. It is well known from available data that the addition of a reinforcement to aluminum and aluminum alloys increases the wear resistance and also produces an improvement in strength [3-5]. Nevertheless, the drawback of these composites is their high production cost which introduces an effective limitation on many of their potential industrial applications.

The use of powder metallurgy (PM) is one of the most common production techniques in the fabrication of MMCs. Thus, by comparison with casting methods, powder metallurgy provides a better control of the microstructure with improved distributions of second phase particles and generally with an absence of any segregation. Conventional consolidation techniques, such as hot-isostatic pressing and hot pressing, can consolidate powders by the application of both heat and pressure but these conventional methods usually lead to significant grain growth [6, 7].

Among the different techniques of PM developed for the manufacture of MMCs, processing through the application of severe plastic deformation (SPD) stands out as the preferred option for the consolidation of powders, particles and machining chips at ambient or low temperatures. The use of SPD methods overcomes many of the difficulties related to impurities and residual porosity in compact samples [8].

It is well documented that the use of heavy cold deformation, as in cold rolling, extrusion and drawing, introduces a significant microstructural refinement at low temperatures. However, the structures formed are usually subgrains of a cellular type composed of boundaries having low angles of misorientation [9, 10]. By contrast, the structures produced by SPD processing are generally of a severely misoriented fragmented type made up of boundaries containing primarily high angles of misorientation [11].

Special methods of SPD were developed and used for the consolidation of metallic powders and MMCs and these methods are High-Pressure Torsion (HPT) [12, 13], Equal Channel Angular Pressing (ECAP) [14, 15] and others.

Using HPT is an effective tool for the consolidation of metal powders and MMCs at room temperature to obtain densely-packed materials. In the HPT process, a disk sample is placed between two anvils rotating under a high compressive force and this imposes an extremely high hydrostatic pressure concurrent with torsional straining [16]. The nominal pressure range in the HPT process is normally between 2-8 GPa and this is above the flow stress of most metallic materials. This means that applying a number of revolutions in HPT processing will produce an almost fully-dense bulk solid. The torsional straining of the particles increases their surface areas and this promotes an improved binding between them. In addition, the grains are refined, thereby producing unique microstructures with unprecedented strength [17, 18]. For example, an Al-10 wt.% Fe alloy was consolidated from high purity elemental powders at room temperature using HPT at a pressure of 6 GPa and the relative density of the consolidated disks

was >99% even at low total strains [19]. More recently, it was reported that coarse-grained aluminum powder of 99.5 wt.% purity was consolidated by HPT at room temperature and after 4 turns with a pressure of ~1.2 GPa a relative density of 99.83% was achieved [20].

There are now several studies documenting the consolidation of powders by HPT for the production of MMCs. For instance, Al-30vol.% Al_2O_3 composite HPT disks were produced by 10, 20 and 50 turns at 6 GPa [21]. Also, an aluminum matrix composite reinforced by graphene platelets, 0.25 wt.% and 0.5 wt.%, was consolidated by HPT under an applied pressure of 3 GPa for 10 revolutions at room temperature [22] and similarly Al powder was consolidated with 5 wt.% of graphene nanoplates using a pressure of 6 GPa for up to 20 turns at room temperature [13]. Ultrafine-grained Al-based composites with 10 and 20 vol.% of Al_2O_3 were produced by cold consolidation of powders using HPT under a pressure of 1.5 GPa for 10 turns and these samples were used to analyze the wear resistance and tribological features [23].

Nevertheless, despite the great potential of producing Al-based MMCs by HPT powder consolidation, most reports in the literature are related to the use of pure Al as matrix material [13,19-23]. Very little attention has been given to powder consolidation by HPT for the production of MMCs having a high strength aluminum alloy matrix reinforced with ceramic particles. Recent research showed that HPT processing of an aluminum alloy 7075 reinforced with 10 vol.% Al_2O_3 improved the hardness significantly and introduced a superplastic capability [24] but this MMC was processed from a bulk sample. Therefore, the present research was initiated with the objective of producing an MMC using a high strength Al 7050 alloy matrix reinforced with 10% vol. Al_2O_3 by using HPT as the consolidation method without any prior sintering.

2. Experimental materials and procedures

Al 7050 machining chips were collected from the manufacture of aircraft components and then used for further gas atomization. The chemical composition of the machining chips, as

determined by inductively coupled plasma optical emission spectrometry (ICP-OES), was (in wt.%) 5.97% Zn; 1.96% Mg; 2.25% Cu; 0.07% Zr; 0.08% Fe; 0.02% Si, as described in an earlier report [25]. The gas-atomized Al 7050 alloy powder was then mixed with a 10% volume fraction of Al_2O_3 powder. The volume fraction was chosen based on other reports of Al-based MMC processed by HPT [23,24]. The Al_2O_3 particle size is ~1μm. The atomized Al 7050 powder was not sieved, then a mixture of powders ranging from ~20 μm to ~500 μm was used in this study. The powders were hand mixed in a crucible for 10 min.

The product was pre-compacted at room temperature using a uniaxial pressure of ~250 MPa into a 10 mm diameter disk with a thickness of ~1.0 mm. The pre-compacted disk was then processed by HPT at room temperature using a quasi-constrained facility [26] where the disk underwent a nominal pressure of 6.0 GPa with a rotation speed of 2 rpm. The rotation was terminated after 50 turns (N = 50). The final thickness of the disk was around 0.8 μm. The consolidated MMC was then characterized by scanning electron microscopy (SEM), X-ray diffraction (XRD) transmission electron microscopy (TEM) and the mechanical properties were evaluated using Vickers microhardness testing.

The upper surface of the as-HPT processed disk was ground and polished to a mirror-like surface without chemical etching for further analysis by SEM using a JEOL 6360LV operating at 15 kV with backscattered electron imaging. Chemical analysis was performed by energy-dispersive X-ray spectroscopy (EDS) coupled to the SEM using an X-ray Dispersive Energy Spectrometer THERMO NORAN Quest. The XRD measurements were carried out with a PANalytical Empyrean diffractometer using 30 kV voltage, 30 mA current, a 2θ interval of 20°-90° at 50 steps per degree and a count time of 1 second per step. For TEM, the sample was prepared by the Focused Ion Beam (FIB) technique using a Quanta FEG 3D FEI which allowed cutting and thinning of a small lamella with micrometric dimensions. The lamella was extracted at a radial distance of ~4 mm from the disk center exactly in the middle of the disk thickness.

The lamella was around 4 × 5 μm^2. The TEM was operated at 200 kV using a TECNAI G2-20 SuperTwin FEI. The grain size was determined by measuring the grain mean diameter in the TEM images. Microhardness testing was performed with a load of 1 kgf and a dwell time of 10 s for each indentation. For the construction of a color-coded hardness map showing the distribution of hardness values throughout one-quarter of the surface of the disk, microhardness measurements were taken from the disk surface every 0.5 mm in the *X* and *Y* directions between the center of the disk and the edge. The average hardness was obtained from measurements at equal distances from the disk center.

3. Experimental results

Processing of the powder by SPD under HPT straining produced a bulk Al 7050-10 vol.% Al_2O_3 disk. Fig. 1 shows representative SEM images at different magnifications near the center of the disk where the gray portion represents the composite matrix of the Al 7050 alloy and the darker areas correspond to the particles of Al_2O_3. The majority of these particles appear to be agglomerated in some areas and close inspection showed that the agglomerations reached sizes of up to tens of microns in the center of the disk. The total area fraction (determined using image analysis) of particles calculated for the entire disk was ~11% which is in excellent agreement with the 10% volume fraction of Al_2O_3 powder used in the sample preparation. Fig. 1 (c-d) shows more thoroughly segregated white particles which may be the result of the formation of second phases during the solidification of the powder during the atomization, such as the hardening phase η' or the overaged η. Both phases are normally present in this system of alloy.

Examining more closely Fig. 1 (a), it is also evident that there are some bright particles. An EDS analysis of these particles is summarized in Table 1 and it reveals they are rich in Fe, Nb and Cr. Although care was taken to avoid any contamination during the sample preparation, it appears that some impurities may have become absorbed during the processing steps associated

with the collecting and cleaning of the machining chips, the gas atomization, and the consolidation and HPT processing. However, the number density of these particles is significantly smaller than for the alumina particles or second phase precipitates. Therefore they are expected to play only a minor role in microstructural evolution and hardness. The hardness testing was not conducted at or close to these particles in order to reduce their influence on the hardness data.

Fig. 2 shows SEM images from the edge of the disk. Comparing Fig. 1 and Fig. 2, it is apparent that the size of the dark contrast areas, which correspond to the Al_2O_3 particles, is smaller near the edge than in the center. At the periphery of the disk, the Al_2O_3 particle size varied from ~20 μm to less than 10 μm and the area fraction of particles calculated at the edge was ~9%. The EDS map on Fig. 2 (b) evidences the presence of the Al_2O_3 particles

Table 2 summarizes the result of the EDS analysis at these small segregated white particles. The result demonstrates there is a significant presence of elements such as Zn, Cu and Mg, and the weight contents are approximately 11%, 7% and 6%, respectively. If considered with reference to the chemical composition of the machining chips, as described in the preceding section, it is apparent that the content of these alloying elements is considerably higher in the white particles than in the matrix material comprising the bulk of the MMC.

Fig. 3 shows XRD patterns of the disk of the Al 7050-10 vol.% Al_2O_3 composite after processing through 50 turns. A few small peaks associated with the Al_2O_3 were identified in the pattern and are marked by black dots but the well-defined higher peaks refer to aluminum and are identified in the pattern by small gray squares. The small brighter areas observed within the aluminum matrix in the SEM images (Figs. 1 and 2), which are attributed to development of the hardening phase η' or the overaged η, were not detected by XRD because of the small volume fraction of the second phases. However, since the material was not subjected to an aging treatment, the fraction of these phases will be generally very low.

The TEM micrographs and the selected area electron diffraction (SAED) pattern in Fig. 4(a-d) document the grain structure of the Al 7050 matrix after straining by HPT for 50 turns. It is clear that consolidation to a fully-granular structure was accomplished. The grain size was estimated using dark-field image and it was found that there was a broad range of grain sizes of the order of ~50 to ~200 nm. The results provide a clear demonstration that the shear strain was effectively imposed on the Al 7050 matrix so that significant grain refinement was accomplished and with final grain sizes that are much smaller than those generally observed in pure Al [13]. The range of grain sizes observed in the present investigation agrees with reports in the literature of grain sizes of 90 ~ 110 nm in an Al 7075 alloy [27] and 40 ~ 300 nm in an Al 7136 alloy [28]. In addition, a high degree of misorientation of the grains is evident due to the formation of typical Debye diffraction rings in the SAED pattern. It is well established that the general misorientations of the grain boundaries increase with increasing numbers of HPT turns [19]. Careful inspection of Fig. 4a also reveals a different morphology of the grains at different areas of the lamella. Thus, the grains in the upper part of Fig. 4a display an elongated morphology whereas the grains in the lower part are more equiaxed. This is also observed in the dark field image in Fig. 4b. Figures 4c and d show higher magnification images of areas with these different grain morphologies. Elongated grains with widths as thin as ~20 nm are clearly visible in Fig. 4c but less elongated grains having larger widths are present in Fig. 4d.

In order to provide a macroscopic representation of the variations in hardness across one-quarter of the surface of the disk, Fig. 5 shows a color-coded contour map for a disk processed by HPT through 50 turns. As a general overview, the color-coded map confirms there are higher hardness values at the edge of the disk although there is some heterogeneity in the distribution of hardness values. Part of this heterogeneity is probably due to the presence of alumina particles within the aluminum-based matrix. Some areas display a higher density of alumina

agglomerations while other areas display a finer dispersion of these hard particles. Therefore this difference in distribution of hard particles may affect the local hardness.

The hardness values were plotted as a function of the effective strain in Fig. 6 where the effective strain, ε, was estimated from the expression [29,30]

$$\varepsilon = \frac{2\pi N r}{\sqrt{3}h} \quad (1)$$

where *N* is the number of turns, *r* is the distance to the disc center and *h* is the thickness of the sample. All of the experimental points lie along a well-defined line which may be expressed by

$$Hv = 200 * \varepsilon^{0.06} \quad (2)$$

It is well established that the grain refinement is not uniform from the center to the edge of the HPT-processed disk due to the heterogeneous imposed strain. Nevertheless, there are many reports showing that a steady-state condition is reached at which the microstructure and the properties tend to become uniform. [31, 32]. The hardness values obtained after HPT in the present sample are higher than for other samples from the same alloy system. For example, it was shown that the processing of an Al 7150 through 5 turns of HPT gave a maximum hardness at the edge of the disk of ~240 Hv [33]. The hardness values in the present experiments are also higher than reported for a bulk Al 7075-10% Al_2O_3 composite processed to only 20 turns of HPT [24].

4. Discussion

The consolidation of metallic and hard phase powders into bulk samples was previously studied and documented, particularly for the processing of metal matrix composites by HPT [12, 21, 34-36]. The results in this study provide additional evidence that it is feasible to produce bulk nanostructured metal matrix composites of an Al 7050 alloy with 10 vol.% Al_2O_3 by HPT. The sizes of the metal and ceramic particles were in the range of 20 ~ 500 μm and ~1 μm respectively prior to processing. It was reported earlier that finer particles of a reinforcement phase tend to decrease the densification of the composite [37]. When the particle size is

sufficiently small, the inter-particle forces become relatively strong because the van der Waals force prevails between the particle bonding. Therefore, small particles generally inhibit the flowability of the powder, thereby decreasing the filling density and producing cluster formation [37]. The size of the ceramic particles used in the present investigation was ~1 μm and some agglomerations were observed. However, voids were not observed in the microstructure and there was no evidence for any lack of consolidation.

The SEM images of the 50 turns HPT-processed disk show that the average size of the Al_2O_3 particle clusters decreases at the periphery of the disk. This is anticipated from the strain introduced by HPT which is proportional to the distance from the disk center.

It is known that the hardness values in HPT-processed pure Al reach a maximum value at a low strain followed by a steady-state where the hardness remains constant and the microstructure consists of grains having boundaries with high angles of misorientation but containing few dislocations [31]. These high-angle boundaries act as absorption sites for dislocations when their misorientation angles become sufficiently large. Therefore, a steady-state is established in which dislocation generation is balanced by dislocation absorption as the strain becomes intense. The size of the grains in Al-based alloys processed by HPT is significantly smaller than in pure Al due to the effect of the solid solution and the presence of precipitates which block dislocation motion. As a consequence, the saturation in hardness requires larger values of imposed strain and the peak hardness is higher. For example, a grain size of ~110 nm and a peak hardness of ~280 Hv were obtained in an Al 7075 alloy [27] whereas a grain size of ~0.8 μm and a hardness of ~62 Hv were obtained in commercial purity aluminum [38].

It was suggested [12, 21, 22] that the presence of reinforcements in Al composites may further promote grain refinement in the HPT processing by comparison with pure Al. The present results show that the presence of reinforcements in an Al alloy matrix also leads to high

hardness. The maximum hardness obtained in the present experiments of ~300 Hv is higher than reported in other Al 7xxx alloys [27,33]. Nevertheless, this increase in hardness is not attributed to an increased difficulty for dislocation motion as in the Orowan by-pass mechanism because the average distance between the alumina particles is much larger than the matrix grain size in this investigation. Finer alumina particles were not observed within the grains in the TEM images. Therefore, it appears instead that the grain boundaries are the primary barriers for dislocation motion.

Although the hard particles are not expected, therefore, to play the main role as barriers for dislocation motion, it is anticipated that they contribute to the increase in strength by increasing the deformation imposed during HPT processing. It is known that particles may increase the deformation imposed to a material due to local flow heterogeneities [39] and strain gradients [40]. Recent reports have shown that the incorporation of alumina particles also increases the hardness of pure magnesium [17] and a magnesium alloy [41] and the gain in strength was attributed to the increase in strain during HPT. The distribution of hardness in the processed disc in the present investigation demonstrates that areas with higher imposed strain display slightly larger values which confirms that a saturation was not attained despite the large number of HPT turns. Therefore, the incorporation of particles in this research may have contributed to an increase in the imposed strain and the development of a high hardness.

5. Summary and conclusions

1. An Al 7050-10 vol.% Al_2O_3 composite was successfully produced by consolidation of Al 7050 gas-atomized powder with alumina particles using high-pressure torsion at room temperature without any additional heating or sintering. The microstructural evolution was examined by scanning electron microscopy and transmission electron microscopy.

2. Estimates of the average grain sizes in the Al 7050 matrix after 50 turns of HPT gave values in the range of ~50 to ~200 nm. It is shown that the Al_2O_3 particles agglomerate into clusters during processing and these clusters are larger in the central area of the disk and finer at the edge.
3. A high hardness of ~300 Hv was achieved in the HPT-processed composite and this high value is attributed to grain refinement. The presence of hard particles may have contributed to an increase in the strain imposed during HPT.

Acknowledgements

The authors acknowledge the Center of Microsscopy at the Universidade Federal de Minas Gerais (http://www.microscopia.ufmg.br) for providing equipment and technical support for experiments involving electron microscopy. Fabio Milhorato thanks CAPES-PROEX (Coordenação de Aperfeiçoamento de Pessoal de Nível Superior) for a scholarship received during this research. The authors express their gratitude to Prof. Claudio Shyinti Kiminami (DEMa – UFSCar) and Claudemiro Bolfarini (DEMa – UFSCar) for providing powders of the Al 7050 alloy used in this research and to Prof. Pedro H. R. Pereira for the HPT processing of the sample.

References

[1] Sha, G., & Cerezo, A. (2004). Early-stage precipitation in Al-Zn-Mg-Cu alloy (7050). *Acta Materialia*, *52* (15), 4503–4516.

[2] Rometsch, P. A., Zhang, Y., & Knight, S. (2014). Heat treatment of 7xxx series aluminium alloys - Some recent developments. *Transactions of Nonferrous Metals Society of China (English Edition)*, *24*(7), 2003–2017.

[3] Torralba, J. M., Da Costa, C. E., & Velasco, F. (2003). P/M aluminum matrix composites: An overview. *Journal of Materials Processing Technology*, *133*(1–2), 203–206.

[4] Torres, B., Lieblich, M., Ibáñez, J., & García-Escorial, A. (2002). Mechanical properties of some PM aluminide and silicide reinforced 2124 aluminium matrix composites. *Scripta Materialia*, *47*(1), 45–49.

[5] Chawla, N., & Shen, Y. L. (2001). Mechanical behavior of particle reinforced metal matrix composites. *Advanced Engineering Materials*, *3*(6), 357–370.

[6] Rahimian, M., Ehsani, N., Parvin, N., & reza Baharvandi, H. (2009). The effect of particle size, sintering temperature and sintering time on the properties of Al-Al_2O_3 composites, made by powder metallurgy. *Journal of Materials Processing Technology*, *209*(14), 5387–5393.

[7] Alexandrov, I. V., Zhu, Y. T., Lowe, T. C., Islamgaliev, R. K., & Valiev, R. Z. (1998). Consolidation of nanometer sized powders using severe plastic torsional straining. *Nanostructured Materials*, *10*(1), 45–54.

[8] Valiev, R. Z., Islamgaliev, R. K., & Alexandrov, I. V. (2000). Bulk nanostructured materials from severe plastic deformation. *Progress in Materials Science*, *45*, 103–189.

[9] Abbaschian, R., Abbaschian, L., & Reed-Hill, R. E. (2009). Physical Metallurgy Principles (4th ed.). Stamford: Cengage Learning.

[10] Dieter, G. (1988). Mechanical Metallurgy (3rd ed.). London: McGraw-Hill Education.

[11] Valiev, R. Z., Korznikov, A. V., & Mulyukov, R. R. (1993). Structure and properties of ultrafine-grained materials produced by severe plastic deformation. *Materials Science and Engineering: A, 168(2),* 141–148.

[12] Tokunaga, T., Kaneko, K., & Horita, Z. (2008). Production of aluminum-matrix carbon nanotube composite using high pressure torsion. *Materials Science and Engineering A, 490*(1–2), 300–304.

[13] Huang, Y., Bazarnik, P., Wan, D., Luo, D., Pereira P.H.R., Lewandowska, M., Yao, J., Hayden, B.E., & Langdon, T.G. (2019). The fabrication of graphene-reinforced Al-based nanocomposites using high-pressure torsion. *Acta Materialia*, *164*, 499-511.

[14] Balog, M., Simancik, F., Bajana, O., & Requena, G. (2009). ECAP vs. direct extrusion-Techniques for consolidation of ultra-fine Al particles. *Materials Science and Engineering A*, *504*(1–2), 1–7.

[15] Balog, M., Yu, P., Qian, M., Behulova, M., Svec, P., & Cicka, R. (2013). Nanoscaled Al-AlN composites consolidated by equal channel angular pressing (ECAP) of partially in situ nitrided Al powder. *Materials Science and Engineering A*, *562*, 190–195.

[16] Zhilyaev, A. P., & Langdon, T. G. (2008). Using high-pressure torsion for metal processing: Fundamentals and applications. *Progress in Materials Science*, *53*(6), 893–979.

[17] Castro, M. M., Pereira, P. H. R., Isaac, A., Figueiredo, R. B., & Langdon, T. G. (2019). Development of a magnesium-alumina composite through cold consolidation of machining chips by high-pressure torsion. *Journal of Alloys and Compounds*, *780*, 422–427.

[18] Lee, Z., Zhou, F., Valiev, R. Z., Lavernia, E. J., & Nutt, S. R. (2004). Microstructure and microhardness of cryomilled bulk nanocrystalline Al-7.5%Mg alloy consolidated by high pressure torsion. *Scripta Materialia*, *51*(3), 209–214.

[19] Cubero-Sesin, J. M., & Horita, Z. (2012). Powder consolidation of Al-10wt% Fe alloy by high-pressure torsion. *Materials Science and Engineering A*, *558*, 462–471

[20] Khajouei-Nezhad, M., Paydar, M. H., Ebrahimi, R., Jenei, P., Nagy, P., & Gubicza, J. (2017). Microstructure and mechanical properties of ultrafine-grained aluminum consolidated by high-pressure torsion. *Materials Science and Engineering A*, *682*, 501–508.

[21] Ashida, M., Horita, Z., Kita, T., & Kato, A. (2012). Production of Al/Al_2O_3 nanocomposites through consolidation by high-pressure torsion. *Materials Transactions*, *53*(1), 13–16.

[22] Zhao, L., Lu, H., & Gao, Z. (2015). Microstructure and Mechanical Properties of Al/Graphene Composite Produced by High-Pressure Torsion. *Advanced Engineering Materials*, *17*(7), 976–981.

[23] Edalati, K., Ashida, M., Horita, Z., Matsui, T., & Kato, H. (2014). Wear resistance and tribological features of pure aluminum and Al-Al2O3 composites consolidated by high-pressure torsion. *Wear*, *310*(1–2), 83–89.

[24] Sabbaghianrad S., Langdon, T. G. (2016). Developing superplasticity in an aluminum matrix composite processed by high-pressure torsion. *Materials Science & Engineering A*, 665, 36–43.

[25] Mazzer, E. M., Afonso, C. R. M., Galano, M., Kiminami, C. S., & Bolfarini, C. (2013). Microstructure evolution and mechanical properties of Al-Zn-Mg-Cu alloy reprocessed by

spray-forming and heat treated at peak aged condition. *Journal of Alloys and Compounds*, *579*, 169–173.

[26] Figueiredo, R. B., Cetlin, P. R., & Langdon, T. G. (2011). Using finite element modeling to examine the flow processes in quasi-constrained high-pressure torsion. *Materials Science and Engineering A*, *528*(28), 8198–8204.

[27] Zhang, Y., Jin, S., Trimby, P.W., Liao, X., Murshkin, M.Y., Valiev, R.Z., Liu, J., Cairney, J.M., Ringer, S.P., Sha, G. (2019). Dynamic precipitation, segregation and strengthening of an Al-Zn-Mg-Cu alloy (AA7075) processed by high-pressure torsion. *Acta Materialia*, *162*, 19-32.

[28] Duan, Z.C., Liao, X.Z., Kawasaki M., Figueiredo, R.B., Langdon, T.G., Influence of high-pressure torsion on microstructural evolution in an Al–Zn–Mg–Cu alloy. *Journal of Materials Science*, *45*, 4621-4630.

[29] Valiev, R.Z., Ivanisenko, Yu.V., Rauch, E.F., Baudelet, B. (1996). Structure and deformaton behaviour of Armco iron subjected to severe plastic deformation. *Acta Materialia*, 44, 4705-4712.

[30] Jonas, J.J., Ghosh, C., Toth, L.S. (2014). The equivalent strain in high pressure torsion. *Materials Science and Engineering A*, 607, 530-535.

[31] Harai, Y., Ito, Y., & Horita, Z. (2008). High-pressure torsion using ring specimens. *Scripta Materialia*, *58*(6), 469–472.

[32] Xu, C., Horita, Z., & Langdon, T. G. (2007). The evolution of homogeneity in processing by high-pressure torsion. *Acta Materialia*, *55*(1), 203–212.

[33] Ghosh, K. S., Gao, N., & Starink, M. J. (2012). Characterisation of high pressure torsion processed 7150 Al-Zn-Mg-Cu alloy. *Materials Science and Engineering A*, *552*, 164–171.

[34] Tokunaga, T., Kaneko, K., Sato, K., & Horita, Z. (2008). Microstructure and mechanical properties of aluminum-fullerene composite fabricated by high pressure torsion. *Scripta Materialia*, *58*(9), 735–738.

[35] Menéndez, E., Salazar-Alvarez, G., Zhilyaev, A. P., Suriñach, S., Baró, M. D., Nogués, J., & Sort, J. (2008). Cold consolidation of metal-ceramic nanocomposite powders with large ceramic fractions. *Advanced Functional Materials*, *18*(20), 3293–3298.

[36] Asgharzadeh, H., Joo, S. H., & Kim, H. S. (2014). Consolidation of carbon nanotube reinforced aluminum matrix composites by high-pressure torsion. *Metallurgical and Materials Transactions A: Physical Metallurgy and Materials Science*, *45*(9), 4129–4137.

[37] Jiang, G., Daehn, G. S., & Wagoner, R. H. (2001). Inclusion particle size effects on the cyclic compaction of powder composites. *Scripta Materialia*, *44*(7), 1117–1123.

[38] Zhilyaev, A.P., Oh-ishi, K., Langdon, T.G., McNelley, T.R. (2005). Microstructural evolution in commercial purity aluminum during high-pressure torsion. *Materials Science and Engineering A*, *410-411*, 277-280.

[39] Kulagin, R. Beygelzimer, Y., Ivanisenko, Y., Mazilkin, A., Hahn, H. (2017) Modelling of High Pressure Torsion using FEM. *Procedia Engineering*, *207*, 1445-1450.

[40] Fleck, N.A., Muller, G.M., Ashby, M.F., Hutchinson, J.W. (1994) Strain gradient plasticity: Theory and experiment. *Acta Metallurgica et Materialia*, *42*, 475-487.

[41] Castro, M.M., Pereira, P.H.R., Isaac, A., Langdon, T.G., Figueiredo, R.B. (In press) Inverse Hall-Petch behaviour in an AZ91 alloy and in an AZ91-Al_2O_3 composite consolidated by high-pressure torsion. *Advanced Engineering Materials*.

Tables captions:

Table 1 – EDS analysis of small segregated white particles indicating elemental content.

Table 2 - EDS analysis of bright particles indicating their element content and Fe contamination.

Figures captions:

Fig. 1. SEM images of the microstructure of the surface near the center of the disk at different magnifications; the yellow contour indicates the zoom area for the following image.

Fig. 2. (a) SEM micrograph of the microstructure of the surface near the edge of the disk; (b) EDS map corresponding to the micrograph in (a) showing Al and O in the red clusters Fig. 3. X-ray diffraction patterns of the sample processed by 50 turns of HPT.

Fig. 4. TEM micrographs showing microstructure (a,b) with the dark field image obtained from the diffracted beam and the corresponding SAED pattern and (c,d) with different grain morphologies.

Fig. 5. Color-coded contour map showing distribution of microhardness over one-quarter surface of the disk processed for 50 revolutions.

Fig. 6. Vickers microhardness plotted as a function of the effective strain.

Tables:

Table 1 - EDS analysis of bright particles indicating their element content and Fe contamination.

Element	Wt.%	At%
Al	0.75	1.63
Si	0.86	1.79
Nb	15.89	9.98
Sb	0.60	0.29
Cr	8.61	9.67
Fe	73.30	76.65
Total	100.00	100.00

Table 2 – EDS analysis of small segregated white particles indicating elemental content.

Element	Wt.%	At%
Mg	5.98	7.37
Al	75.81	84.19
Cu	6.98	3.29
Zn	11.22	5.14
Total	100.00	100.00

Figures:

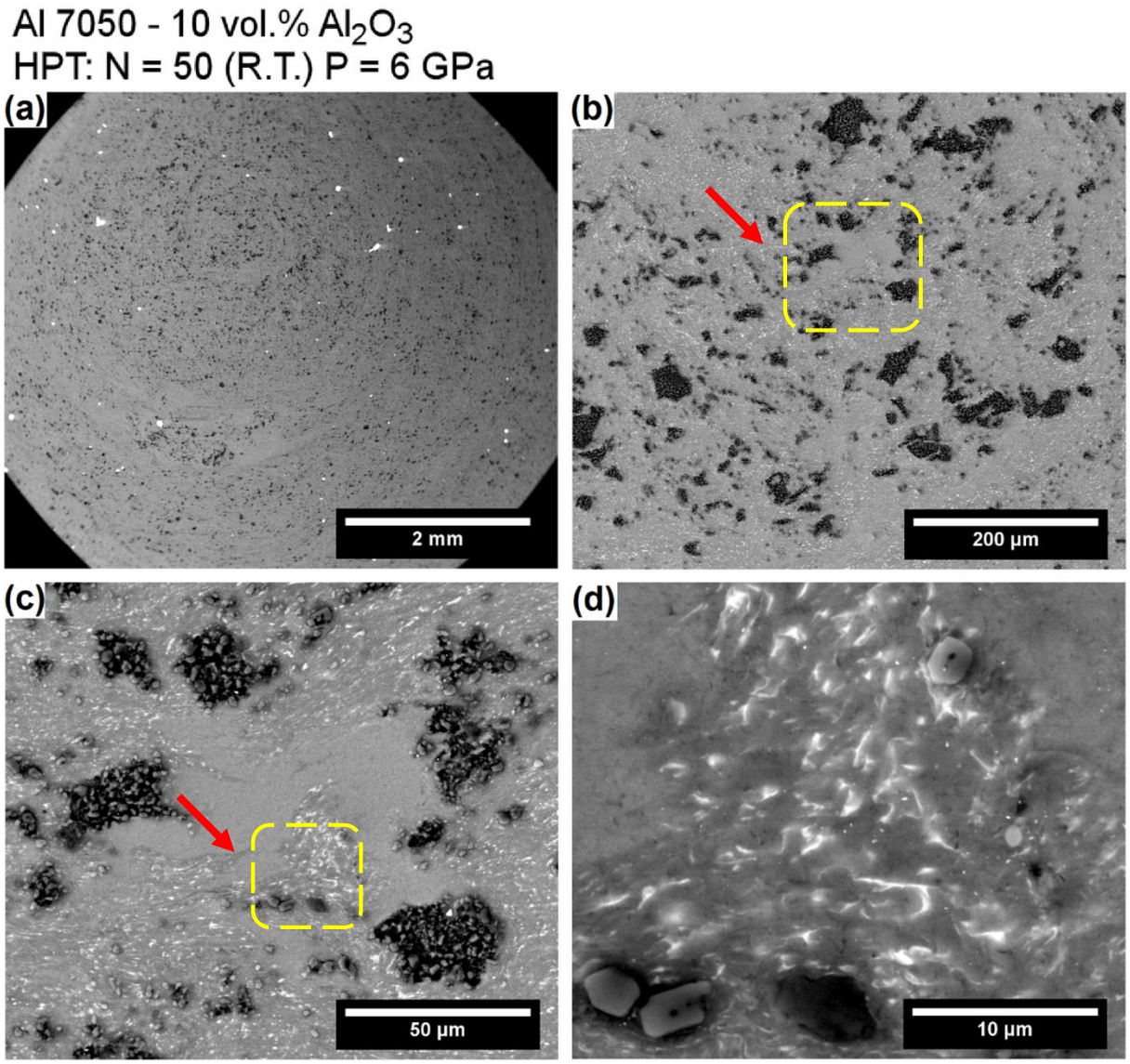

Fig. 1. SEM images of the microstructure near the center of the disk at different magnifications showing evidence of (a) minor contamination (bright spots), (b-c) agglomeration of alumina particles (dark spots) and (d) second phase precipitates; the yellow contour indicates the zoom area for the following image.

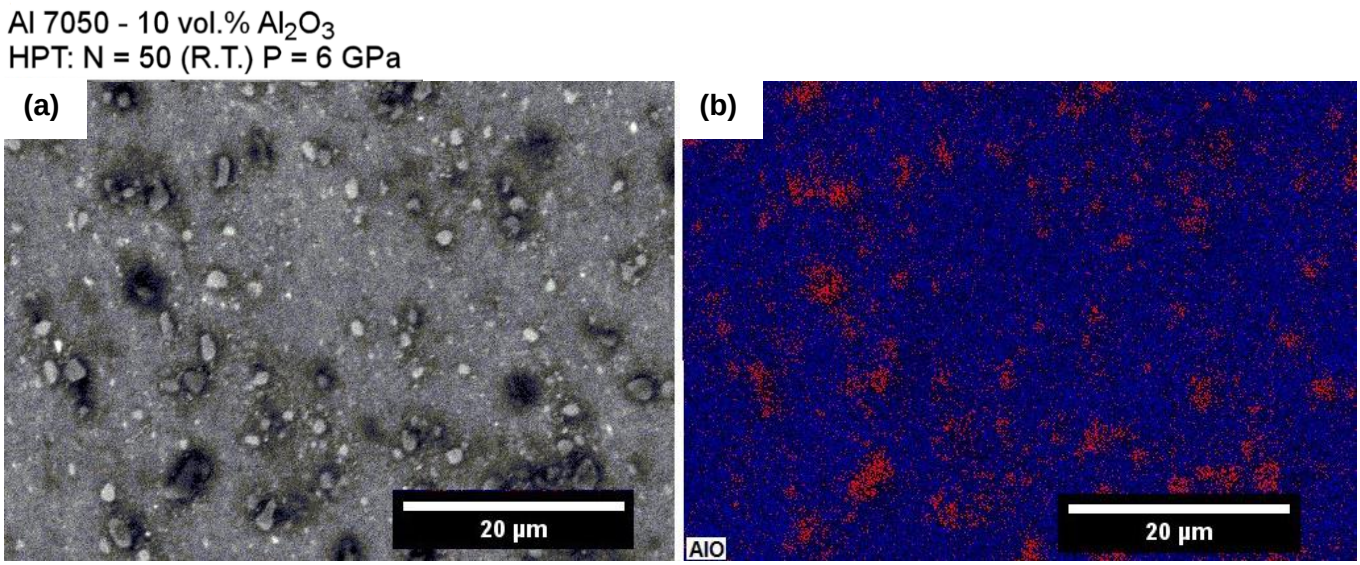

Fig. 2. (a) SEM micrograph of the microstructure of the surface near the edge of the disk; (b) EDS map corresponding to the micrograph in (a) showing Al and O in the red clusters.

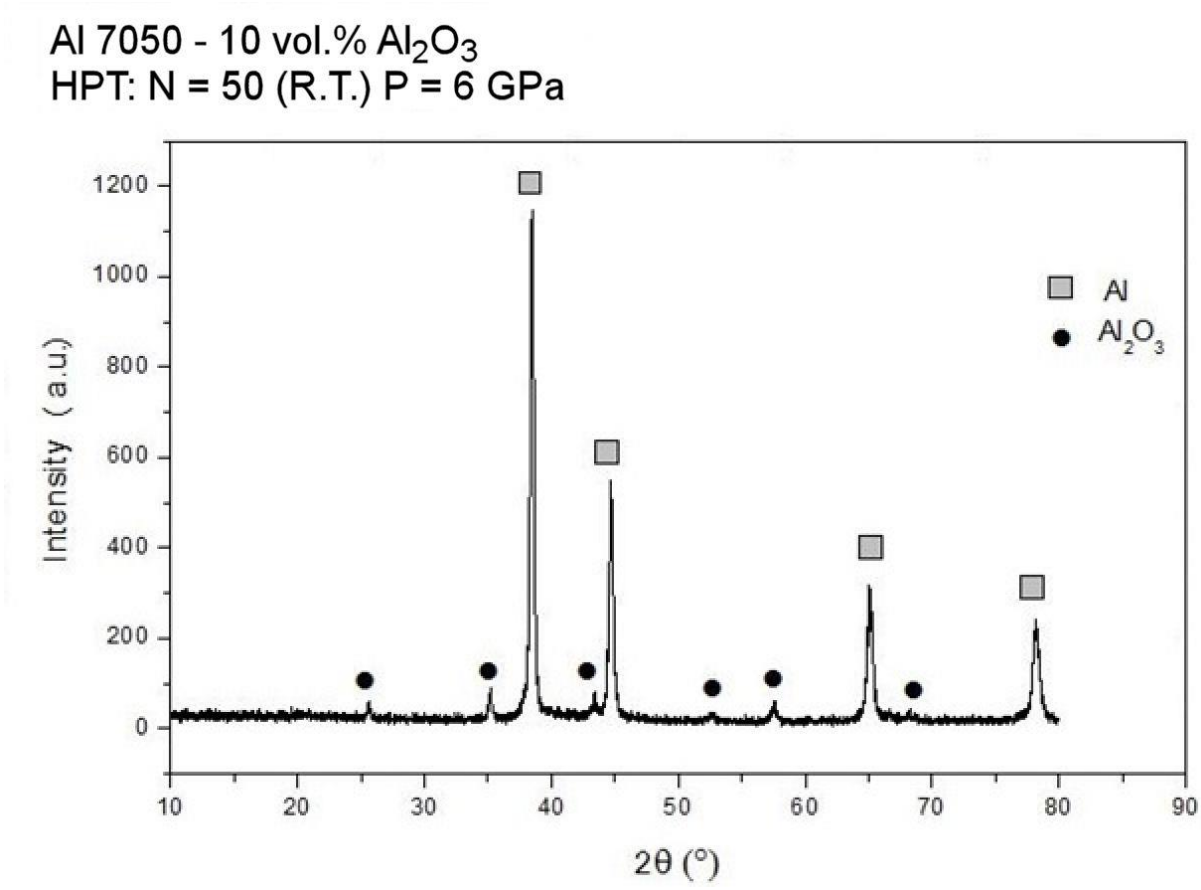

Fig. 3. X-ray diffraction patterns of the sample processed by 50 turns of HPT.

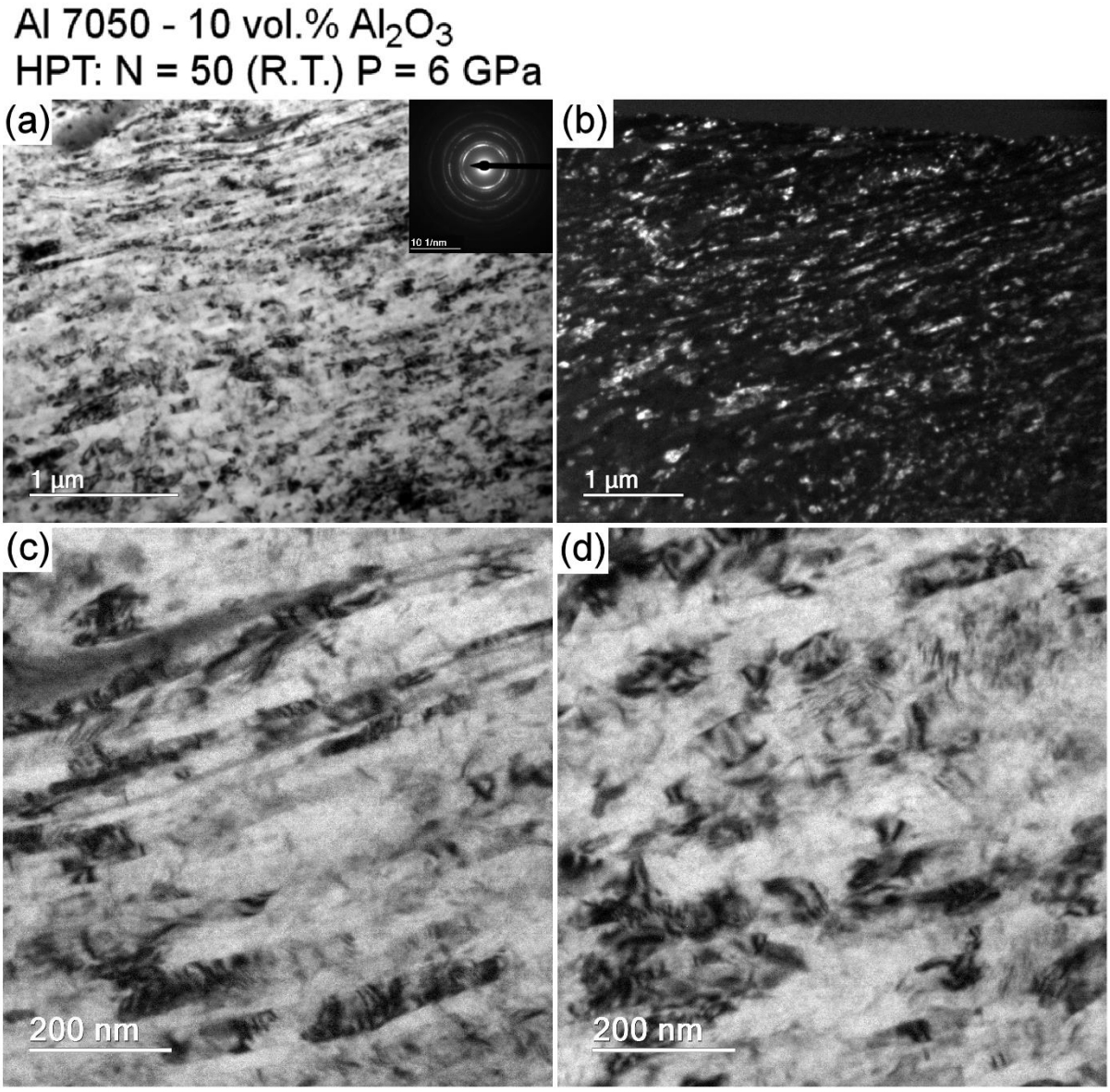

Fig. 4. TEM micrographs showing (a) general grain structure and SAED pattern, (b) dark field image and higher magnification images of regions with (c) elongated grains and (d) less elongated grains.

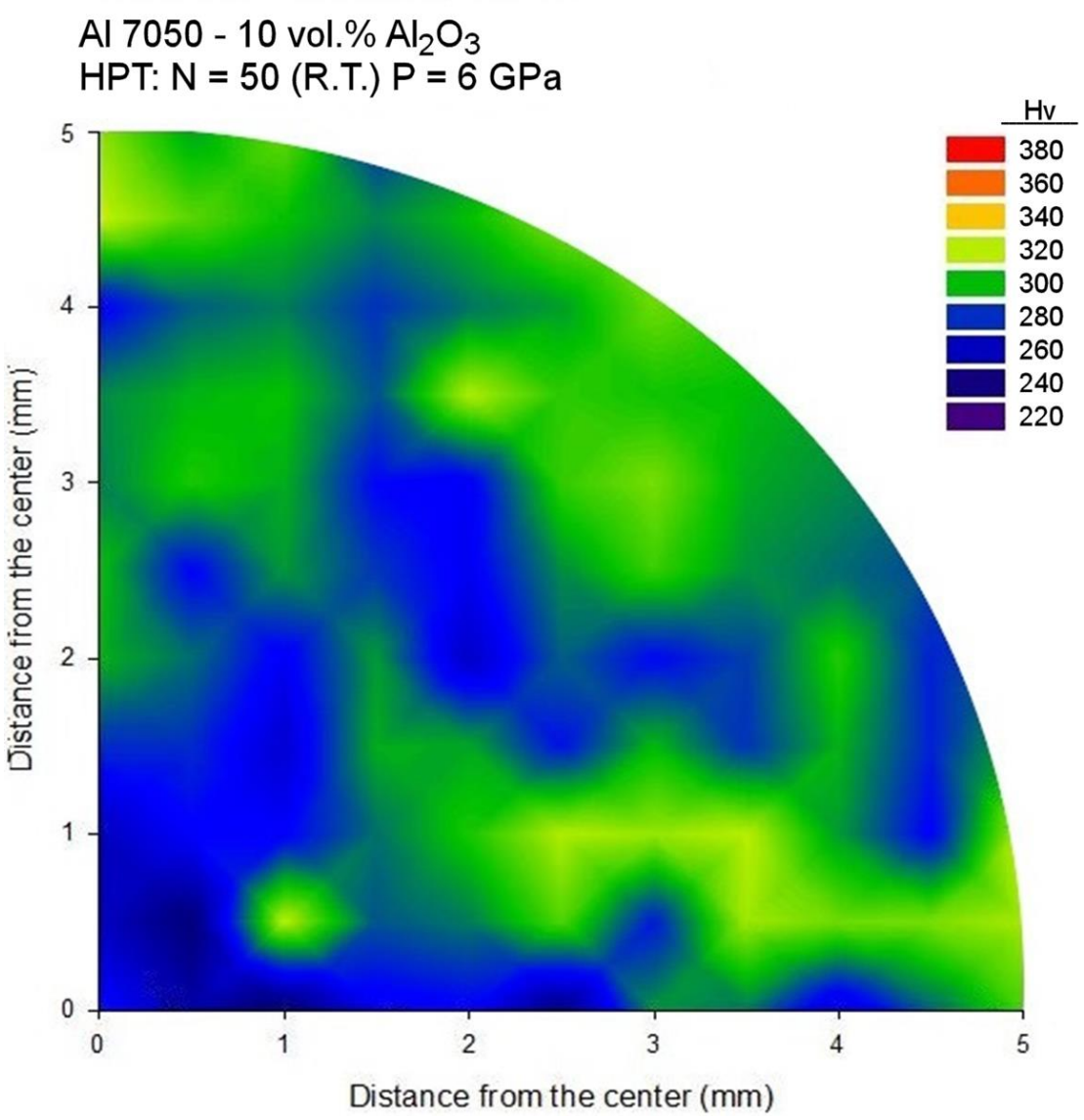

Fig. 5. Color-coded contour map showing distribution of microhardness over one-quarter surface of the disk processed for 50 revolutions.

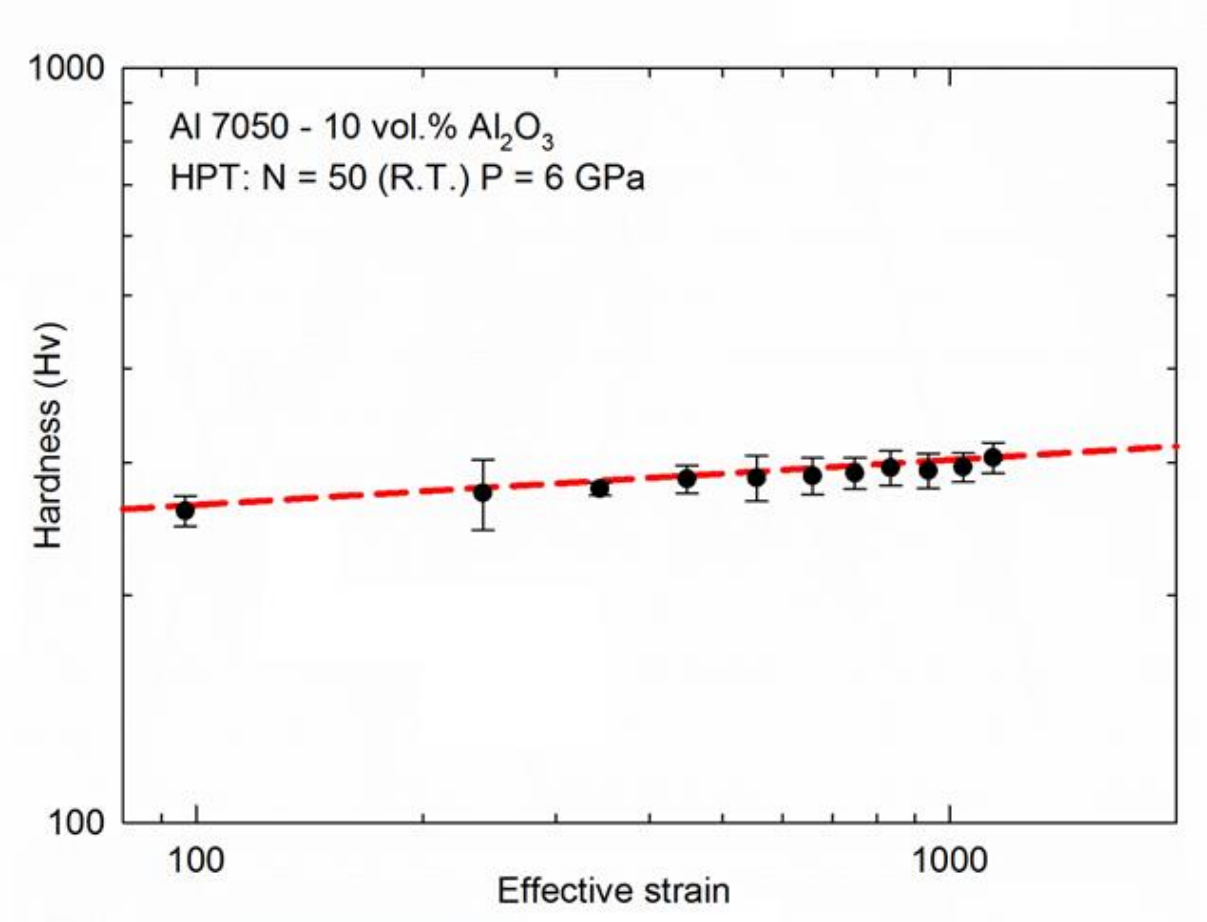

Fig. 6. Vickers microhardness plotted as a function of the effective strain.